

Trends in the Reactivity of Proximate Aluminum Sites in H-SSZ-13

Ashley T. Smith[§], Philipp N. Plessow^{§,*}, Felix Studt^{§,#}

[§] Institute of Catalysis Research and Technology, Karlsruhe Institute of Technology, Hermann-von-Helmholtz-Platz 1, D-76344 Eggenstein-Leopoldshafen, Germany.

[#] Institute for Chemical Technology and Polymer Chemistry, Karlsruhe Institute of Technology, Karlsruhe 76131, Germany

methanol-to-olefin reaction • zeolites • reaction mechanisms • density functional theory • catalysis

ABSTRACT: The reactivity of acidic zeolites with close Al-pairs was investigated using density functional theory. Different spatial distances as well as relative orientations of the two Al atoms were considered. Adsorption of methanol as well as ammonia was computed and shown to be correlated. Additionally, reaction barriers for the stepwise and concerted mechanism of the dehydration of methanol to DME were computed. These barriers were found to correlate well with the adsorption energy of ammonia as a descriptor. This correlation reduces some of the stronger deviations observed in apparent activation barriers, when computing intrinsic barriers referenced to an adsorbed species. Excluding nearest neighbors Al-pairs that violate Löwenstein's rule, the effect of different Al-pair distributions is found to influence apparent activation barriers typically by less than 20 kJ/mol with a mean absolute deviation of 7 kJ/mol.

INTRODUCTION

Zeolites are microporous solid acid catalysts with widespread use in the chemical industry for processes such as fluid catalytic cracking,¹ toluene disproportionation,² dimethyl ether synthesis³ and methanol to hydrocarbon processes.⁴⁻⁷ They are built from [SiO₄]⁴⁻ tetrahedra that are connected via the oxygen atoms resulting in microporous structures with a large variety of different topologies. Substitution of one Si⁴⁺ with a trivalent heteroatom (typically Al³⁺, but others such as Fe³⁺ or Ga³⁺ are also sometimes used) creates a charge imbalance that leads to an acid site if compensated by a proton. In acid-base catalysis, the strength of this acid site as well as the influence of the confinement surrounding it is responsible for the activity of the zeolite for a given reaction.

The gross cumulative activity of zeolites is often complicated by the fact that there are several tetrahedral Si⁴⁺ sites where substitution with Al³⁺ can take place. This leads to multiple acid sites all with different acid strengths, that can vary by as much as 40 kJ/mol if measured through the ammonia heat of adsorption as recently shown by density functional theory (DFT) calculations for the commonly used H-ZSM-5.⁸ Similarly, activation barriers for direct DME-formation were shown to vary by up to 40 kJ/mol, depending on the location of the acid site.⁹ H-SSZ-13, exhibiting the chabazite (CHA) framework topology is less complicated as all 36 tetrahedral Si⁴⁺ positions are crystallographically equivalent such that there is only one unique acid site location possible. Yet, the number of possible isomers becomes increasingly large when substitution of more than one Si⁴⁺ has to be considered. This leads to H-

SSZ-13 being a rather well-defined catalyst for high Si/Al ratios (as there is a small likelihood of more than one aluminum per unit cell), that becomes rather poorly defined for lower Si/Al ratios.

One of the central questions is thus how the proximity of a second aluminum within the framework influences the activity of the acid site. Recent advances in synthesis and characterization of zeolites allow to control the proximity of aluminum atoms to a larger extent,¹⁰⁻¹¹ but it is still difficult to investigate the influence of proximity on the intrinsic activity experimentally. Experimentally, rates for DME-formation were shown to correlate with the number of proximate Al-pairs in H-SSZ-13.¹¹ Quantum chemical calculations, on the other hand, can address these questions directly and are nowadays routinely used to investigate reaction mechanisms in zeolite catalysis.^{9, 12-23} In an investigation of ethanol and methanol dehydration in H-SSZ-13 with varying densities of Al-atoms, variations of activation barriers on the order of 20 kJ/mol were observed for proximate Al-pairs.²⁴

In this contribution we use periodic DFT²⁵⁻²⁶ calculations to investigate the influence of a second aluminum substitution per unit cell as a function of its proximity and to correlate the observed reactivity with measures of acidity. For simplicity we use H-SSZ-13 as there is only one crystallographically distinct position for the first aluminum substitution. We chose dimethyl ether (DME) synthesis from methanol as an example as this reaction has been investigated in great detail both experimentally²⁷⁻²⁸ and theoretically.^{9, 27-36}

METHODS

DFT calculations were performed in a similar manner as in our previous work.³⁷ Briefly, we used the VASP program package³⁸⁻³⁹ in version 5.4.1 with the standard VASP-PAW potentials. The PBE⁴⁰ density functional with the D3 dispersion correction (zero damping) from Grimme⁴¹ (PBE-D3) has been employed. The Brillouin zone was sampled at the Γ point. A Gaussian smearing with a width of 0.1 eV was used. The cutoff energy for the plane waves was 400 eV, 800 eV have been used for the optimization of the unit cell. The lattice constants were optimized for the purely siliceous zeolite and the obtained lengths of the lattice vectors of the unit cell of H-SSZ-13 are 13.625, 13.625 and 15.067 Å, as also used in earlier theoretical studies.¹⁸ The lattice constants were kept fixed at these values in all subsequent calculations. All structures have been fully relaxed and the convergence criteria for SCF cycles and geometry optimization were 10^{-8} eV and 0.01 eV/Å, respectively. The transition states were optimized using automated relaxed potential energy surface scans (ARPESS).⁴² All total energies and Cartesian coordinates are provided as supporting information. Harmonic force constants were computed from a central finite difference method where the oxygen at which the reaction occurs as well as the adjacent T-atoms were included. All transition states were verified to contain only one imaginary frequency corresponding to the transition vector of the reaction. In addition, the connectivity of transition states was confirmed through small displacement along the transition vector followed by optimization to the corresponding minima.

RESULTS AND DISCUSSION

Substitution of Si by Al in acidic zeolites is balanced by the introduction of a proton as shown schematically in Figure 1a. Since every Al-atom is bound to four oxygen atoms, there are always four different binding positions for the proton. We have generally only considered the most stable proton position, since we expect that rapid equilibration of these isomers is possible in the presence of methanol or water.

The separation of a pair of two Al-atoms in an acidic zeolite is illustrated in Figure 1a and we will use the nomenclature P_n to refer to a structure, in which the two closest Al-atoms are n -nearest neighbors. Alternatively, one can say that the two Al atoms are separated by $n-1$ (Si-O)-units. In the employed model of H-SSZ-13 with one aluminum substitution per unit cell (Si/Al ratio of 35), two Al atoms (in two adjacent unit cells) are separated by five (Si-O) units. We will use this P6-structure with one Al per unit cell as the “large separation limit” and will reference the stability and reactivity of closer Al-pairs relative to this limit.

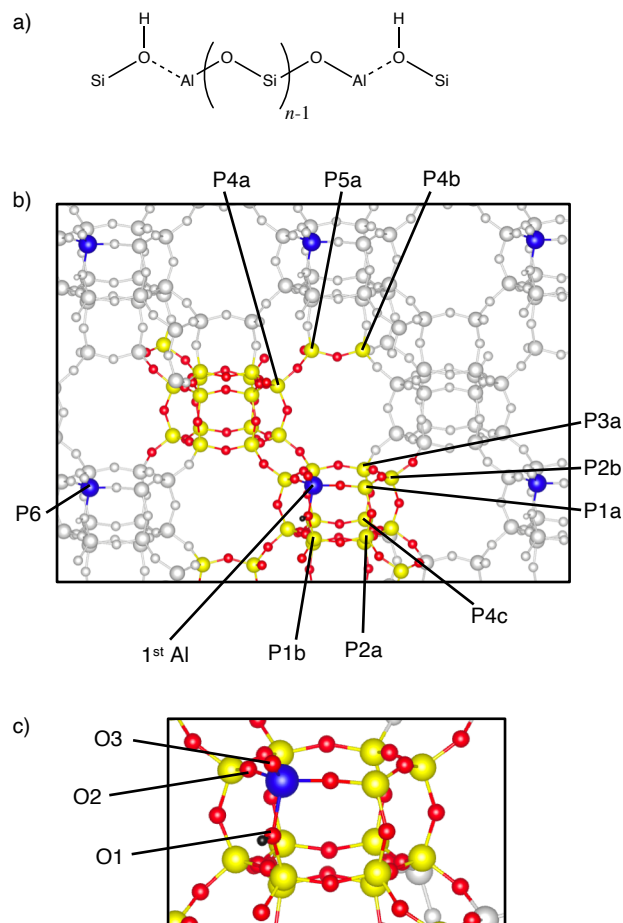


Figure 1. a) Relative position of two n -nearest neighbor aluminum atoms, starting from direct neighbors ($n = 1$), where no intermediate (-O-Si-) group is present to $n = 6$, which is the situation of an isolated Al atom per unit cell. b) Periodic structure of H-SSZ-13 with one Al per unit cell (shown in blue). Silicon and oxygen atoms within the first unit cell are shown in yellow and red respectively and in gray outside of the first unit cell. c) The oxygen atoms bound to the central Al-atom at which the reactivity studied in this work occurs are numbered according to decreasing stability of the clean acid site. The relation of crystallographic labels is given in Table S1 of the SI ($O_1 \rightarrow O_4$, $O_2 \rightarrow O_3$, $O_3 \rightarrow O_2$, $O_4 \rightarrow O_1$).

We will now introduce the second aluminum substitution in H-SSZ-13 (nominal Si/Al ratio of 17). This is illustrated in Figure 1b, where potential positions of an additional second Al atom per unit cell are highlighted. There exist typically numerous different isomers for substitution in a certain distance to the first Al atom. For example, for the substitution directly adjacent to the first Al atom, there are four different positions, which we labeled P1a, P1b, P1c and P1d and analogously for the other positions (see SI for full list and cartesian coordinates of all structures).

We always label the structure according to the closest Al-pair, where the closest Al-atom is not necessarily in the same unit cell, but can also be in a periodic image of the unit cell. Taking this into account, the most distant Al-pair achievable with two Al atoms per unit cell is P5, a fifth-nearest neighbor substitution. Not taking into account

symmetry, substitution of the remaining 35 Si atoms in the 36T unit cell gives rise to 35 additional structures. Overall, there are four P1 isomers, nine P2 isomers, 12 P3 isomers, eight P4 isomers and two P5 isomers. In addition, there are four possible locations for the proton to bind to the connecting oxygen atoms at each acid site, where we have always only considered the most stable one. We label the oxygens in terms of the stability of the proton location of the clean structure (Fig. 1c). This relates to the crystallographic labels as shown in Table S1 ($O_1 \rightarrow O_4$, $O_2 \rightarrow O_3$, $O_3 \rightarrow O_2$, $O_4 \rightarrow O_1$, i.e. the O_1 - O_4 and O_2 - O_3 labels are pairwise exchanged). We investigated all possible variations (see SI) and calculated the stability of the zeolites relative to our reference catalyst P6 according to:

$$\Delta E_{\text{form}} = E(\text{Pn}) + E(\text{oAl}) - 2E(\text{P6}) \quad (1).$$

where $E(\text{Pn})$ is the total energy of the structure with two Al atoms per unit cell under consideration, $E(\text{oAl})$ is the total energy of an unsubstituted, purely siliceous zeolite and $E(\text{P6})$ is the total energy of a zeolite substituted with one Al atom. We find that there is a considerable spread in formation energies with structures being more (by up to 40 kJ/mol) and less (by up to 10 kJ/mol) stable when compared to P6 using equation 1. Interestingly, there are four structures that are more stable than P6 while violating Löwensteins rule ($n = 1$). While a general understanding of the stability of the various zeolites is out of the scope of this study, we note that similar observations have been made in earlier studies.^{24, 43-50} For the 35 different ways in which two Al atoms can be arranged in the unit cell there are in each case 16 different isomers arising from the possibilities to distribute the two protons among the four oxygens bond to each Al atom. The stability of the resulting 540 structures is shown in black in Fig. 2. Out of the 35 possible Al-pairs, we chose a subset of 10 structures that includes all different pair-distances with $n = 1 - 5$ and consists of both stable and unstable distributions according to equation 1 (see SI). Figure 2 shows the stability of these 10 structures in blue, where only the most stable of the 16 possible isomers arising from different proton distributions are shown.

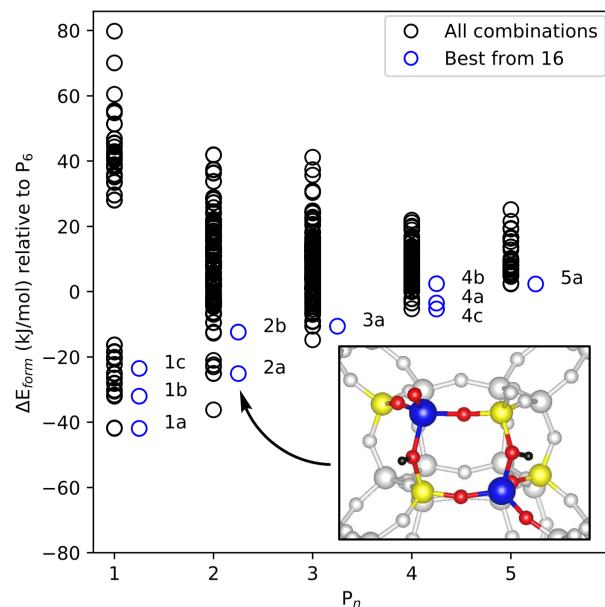


Figure 2. Stability of Al-pairs as a function of distance. The energy is given relative to P6, e.g. the structure where the two Al-atoms are separated by 5 (Si-O)-units. All possible permutations are shown in black and the ten chosen Al-pairs are shown in blue. For these ten pairs, only the most stable arrangement of the two protons in the 16 possible combinations is shown.

We will now discuss the potential energy diagram of the reaction of two methanol to DME, which can proceed via either the associative or dissociative mechanism, see Fig. 3.²⁸ In the former, two methanol molecules adsorb on the acid site(s) and react in a concerted manner to produce DME and water. The latter occurs via two steps, (1) methanol adsorption followed by formation of a surface methoxy species (SMS) and water and (2) reaction of the SMS with a second methanol to DME and the acid site. While the associative mechanism has an overall lower enthalpic barrier, the transition state has a larger entropic penalty and the preferred reaction mechanism hence depends strongly on the temperature. DME synthesis has been subject to numerous theoretical studies employing DFT.^{9, 27-36} We recently showed that transition states calculated with DFT, and PBE-D3 in particular, often have large errors when compared to higher level methods.¹⁸ For example the barrier for direct DME formation calculated with PBE-D3 is underestimated by 37 kJ/mol when compared to CCSD(T)³⁷ calculations. We stress here, however, that we are interested in trends imposed by aluminum proximity rather than absolute accurate numbers, and that trends have been shown to be rather well-preserved at the GGA-DFT level of theory with errors of less than 5 kJ/mol,⁵¹ and we hence stick to PBE-D3 for our investigations here.

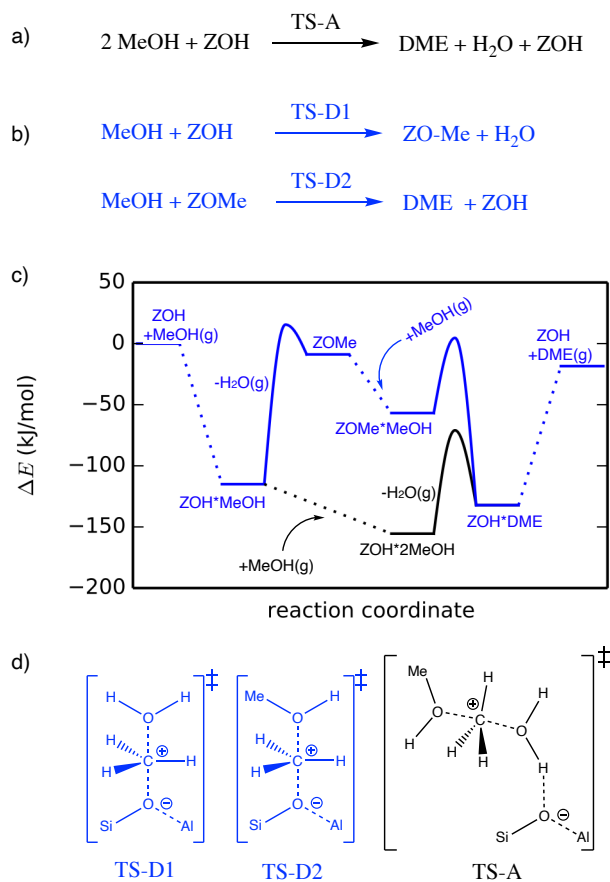


Figure 3. a) associative and b) dissociative mechanism for DME-formation. c) Potential energy diagram of dimethyl ether synthesis from methanol as calculated for H-SSZ-13 with a Si/Al ratio of 35, our reference catalyst (P6). The black and blue pathways correspond to the associative and dissociative mechanism, respectively. All energies are referenced to the empty zeolite and two methanol molecules in the gas-phase at 0 K. An asterisk denotes an adsorbed species at either the acid site (ZOH) or the surface methoxy species (SMS). d) Illustration of the transition states in a-c).

We now turn to calculations of the reaction mechanism presented in Figure 3. We calculated the corresponding energy profile for the 10 different zeolites considered herein. For each structure, all four isomers arising from permutations of the proton at the second acid site were computed explicitly and only the most stable structure is reported. Figure 4 shows the transition state energies for SMS-formation in comparison to that calculated for P6, both relative to gas-phase methanol (apparent barriers) as well as the initial state (intrinsic barriers), that is pre-adsorbed methanol. In this work, apparent barriers are always referenced to gas phase methanol and intrinsic barriers are referenced to a single adsorbed methanol, which refers to the high temperature limit, where the methanol coverage is negligible. In these calculations, SMS formation is studied separately at different oxygens. As described above, all four proton locations at the second acid site are explicitly computed and only the most stable structure is considered. The different oxygen positions are shown in Fig. 1c.

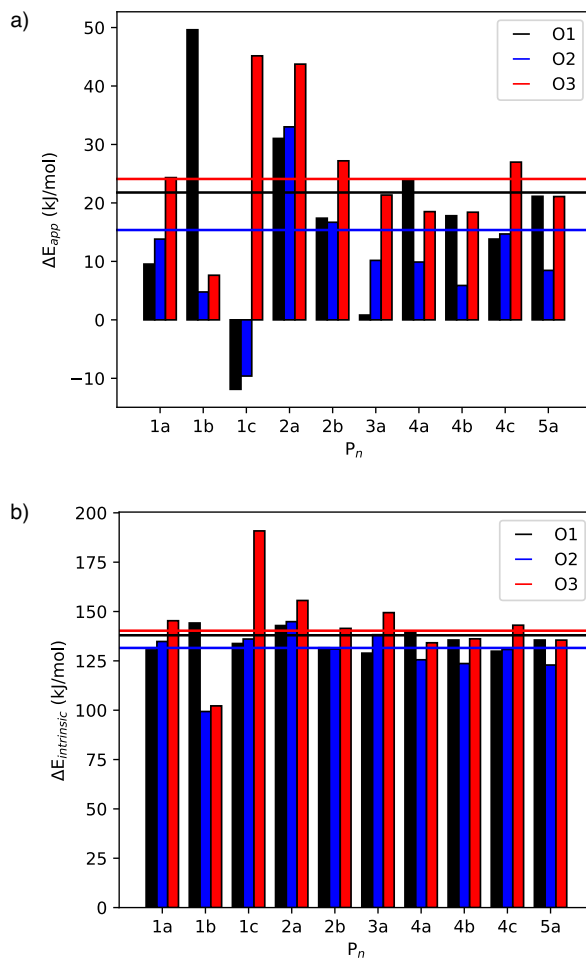


Figure 4. a) Apparent and b) intrinsic activation energies for SMS formation for selected Al-pairs. SMS formation at three different oxygens is shown in black, red and blue and the barriers of the distant pair (P6) are shown as horizontal lines. The nomenclature for the oxygen location is illustrated in Fig. 1c.

Structures with nearest-neighbor Al-pairs (in violation of Löwenstein's rule) lead in some cases to relatively low apparent barriers, for example for 1b and 1c. However, very high barriers are observed for reactions occurring at the bridging oxygen (Al-O-Al), i.e. O3 for P1c and O1 for P1b. For the structures that obey Löwenstein's rule, variations in intrinsic barriers are generally below 20 kJ/mol. The fact that the variation in intrinsic barriers is sometimes smaller than in apparent barriers suggests that there is a correlation between transition state energies and the energy for methanol adsorption. Such variations are often explained in terms of the acidity of the zeolite. There are various measures for the acidity of zeolites, such as the deprotonation energy,^{34, 52-53} the O-H frequency shift upon CO adsorption⁵⁴ and the ammonia heat of adsorption, $E_{\text{ads}}(\text{NH}_3)$.⁵⁵⁻⁵⁷ We chose the latter to investigate the effect of aluminum proximity in more detail and to investigate to what extent $E_{\text{ads}}(\text{NH}_3)$ can serve as a descriptor for the zeolites' reactivity. Figure 5 shows the adsorption energy of methanol and the barrier for direct DME-formation as a function of $E_{\text{ads}}(\text{NH}_3)$. In agreement with the investigation of Hoffman et al.,²⁴ we find that substitution of the second

Al across the four-membered ring into a 2nd-nearest neighbor position (P2a, see inset in Fig. 2) leads to a destabilization of the concerted transition state, while substitution across the six-membered ring into a 3rd-nearest neighbor position (P3a, see inset in Fig. 4b) leads to stabilization and in fact to the lowest transition state, not considering nearest neighbor positions.

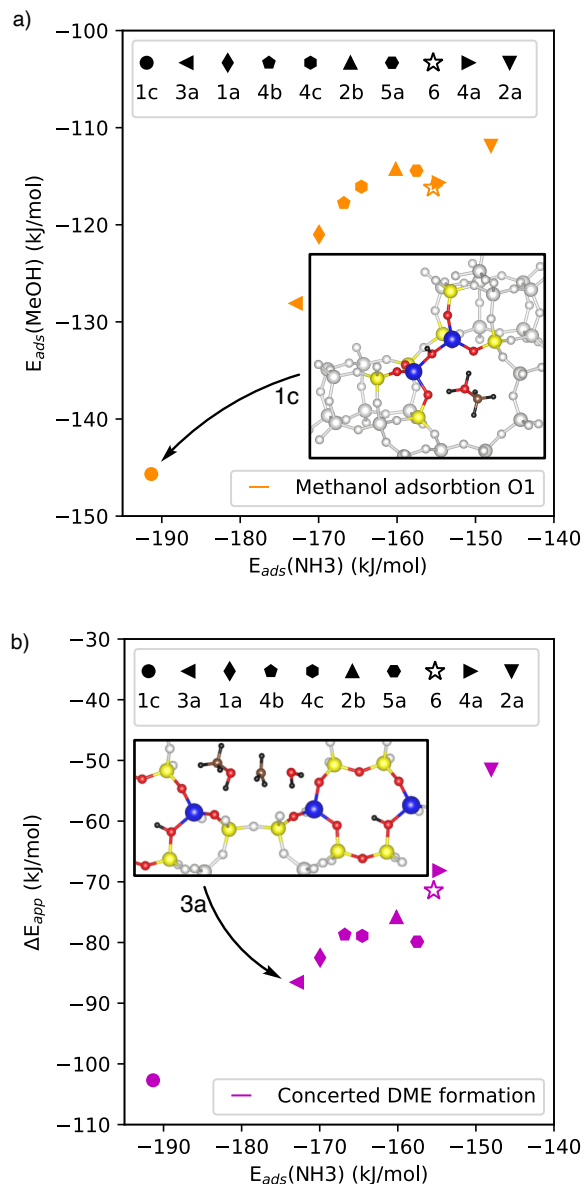


Figure 5. a) Adsorption energies of methanol and b) Apparent activation energies for direct DME-formation for selected Al-pairs as a function of the adsorption energy of ammonia.

Figure 6 shows the transition state energies for the first and second step of stepwise DME formation as a function of $E_{ads}(\text{NH}_3)$. For SMS-formation, the barrier is additionally investigated for formation of the SMS at three different oxygens. As for concerted DME-formation, we observe that the transition state energies largely correlate well with acidity (linear regressions are shown and discussed in section S3 of the SI). Similarly, structures P3a (P2a) are particularly stable (unstable). For isolated acid sites, SMS-

formation is preferred at oxygen O2, where the transition state is located within an eight-membered ring and two hydrogen bonds are formed between water and framework oxygen (see inset in Fig. 6).²⁴ As observed in ref. 24, for the 3rd-nearest neighbor position across the six-membered ring (P3a), the most favorable oxygen for SMS-formation is O1. Due to the more stable methanol adsorption for this Al-pair, the decrease in the apparent activation barrier (-15 kJ/mol relative to P6) does not carry over to the intrinsic barrier (-3 kJ/mol, see also Fig. 2). Similarly, for structure P2a, the apparent barrier deviates more from P6 (+16 kJ/mol) than the intrinsic barrier (+11 kJ/mol).

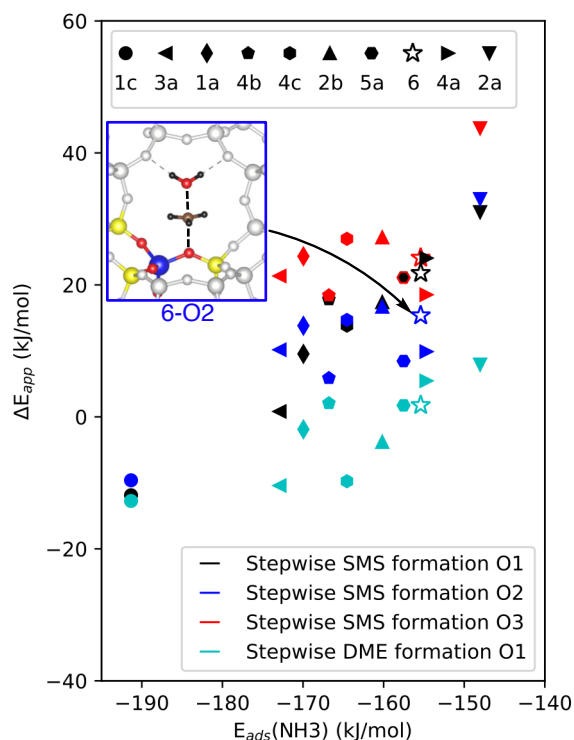


Figure 6. Apparent activation energies for stepwise DME-formation for selected Al-pairs as a function of the adsorption energy of ammonia. (Stepwise SMS formation for O3 for P1c is not shown).

So far, our investigations focused on how the proximity of an aluminum next to the acid site affects its interaction with adsorbates and transition states. However, there may be additional adsorption also on that second acidic proton, which in turn might alter the acidity of the first. In order to shed light onto this issue we repeated the calculations of nine of the transition states shown in Fig. 6, but added an adsorbed methanol to the second acid site. The obtained apparent activation energies are shown in Fig. 7 and compared with those obtained for the free acid site. The effect of the coadsorbed second methanol on the barrier is generally unsystematic and smaller than the difference induced by the Al-pair distribution. The trends between the different Al-pairs therefore remain largely unchanged.

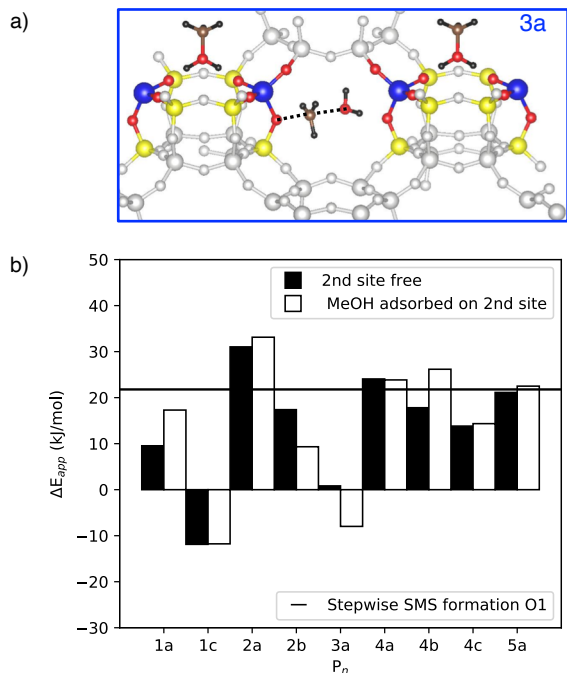


Figure 7. a) Illustration of the transition state for P_{3a} for SMS formation with a coadsorbed MeOH at the second acid site. b) Transition state energies for SMS formation with a second methanol molecule coadsorbed at the second acid site.

All adsorption energies and activation barriers computed in this work are summarized in Fig. 8, which shows a histogram of the deviation of these energies with respect to the most distant pair (P6). The largest differences are observed for nearest neighbor Al-pairs with a mean absolute deviation (MAD) of 16.1 kJ/mol. Importantly, these pairs are not expected to form under usual synthesis conditions, according to Löwenstein's rule. For typical, more distant Al-pairs expected for low Si/Al ratios, the influence of a neighboring Al site is much less pronounced with most deviations within ± 20 kJ/mol, and a MAD of 5.6 kJ/mol. Despite the correlation between adsorption energies and transition states (see Figures 5 and 6), deviations are similar for intrinsic and apparent barriers with a MAD of 5.8 and 7.0 kJ/mol, respectively (excluding nearest neighbor Al-pairs).

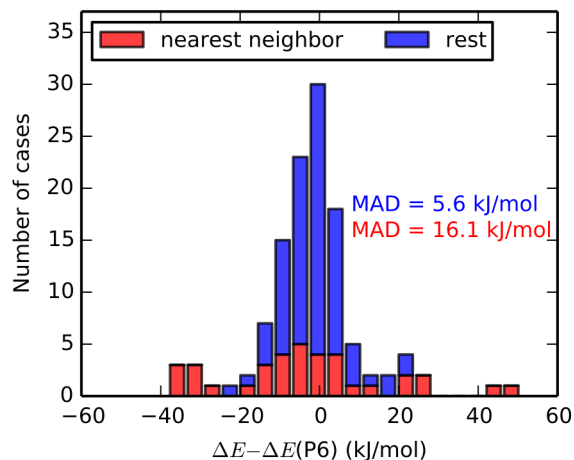


Figure 8. Statistics of the effect of proximate Al-pairs, as measured relative to the adsorption energy, or activation barrier ΔE of structure P6. Nearest neighbor Al-O-Al pairs (violating Löwenstein's rule) are shown in red, the remaining structures are shown in blue. The total height of the two sets of stacked bars corresponds to all structures.

SUMMARY AND CONCLUSIONS

We have investigated the effective of the proximity and spatial orientation of Al-pairs on the reactivity of the zeolite H-SSZ-13. Here we have focused on methanol dehydration to DME as a probe reaction, where we have studied both the concerted (associative) and stepwise (dissociative) mechanism. The effect of Al-pairs on adsorption- and transition state energies was investigated relative to the situation of a single acid site per unit cell (Si/Al ratio of 35), where the Al-atom is separated by five (Si-O)-units from its periodic image. While most changes are in the ± 5 kJ/mol range, there are some notable outliers. The largest variations of up to 50 kJ/mol were found for direct Al-O-Al pairs which violate Löwenstein's rule.

Both adsorption energies and activation barriers of the various Al-pair distributions correlate well with the adsorption energy of ammonia, which we use as a descriptor for acidity. This leads to slight decrease in the variation of intrinsic barriers as compared to apparent barriers. Especially for the particularly reactive (3rd-nearest neighbor across the six-membered ring, P_{3a}) and unreactive substitutions (2nd-nearest neighbor across the four-membered ring, P_{2a}), these trends are diminished in the intrinsic activation barriers.

The commonly applied model of isolated acid site is in most cases a good model for structures obeying Löwenstein's rule, with a mean absolute deviation (MAD) of 5.6 kJ/mol for all adsorption energies and transition states considered. There are, however, noteworthy exceptions where transition states for certain Al-pairs are on the order of 20 kJ/mol more stable. On the other hand, it is often not clear to which extent a specific Al-Al configuration is present in a certain zeolite sample. We therefore believe that the commonly applied computational model exhibiting well separated acid sites (e.g. Si/Al=35 in H-SSZ-13) is

generally a reasonable model giving a good first estimate also for zeolites with smaller Si/Al ratios. Larger deviations (MAD = 16.1 kJ/mol) were found for nearest neighbor aluminum substitutions, e.g. Al-O-Al pairs. These are, however, generally believed not to be formed under standard synthesis conditions according to Löwenstein's rule.

ASSOCIATED CONTENT

Supporting Information

Additional analysis, total energies and Cartesian coordinates of the relevant computed structures.

AUTHOR INFORMATION

Corresponding Author

*plessow@kit.edu

Author Contributions

The manuscript was written through contributions of all authors. / All authors have given approval to the final version of the manuscript.

ACKNOWLEDGMENT

The authors acknowledge support by the state of Baden-Württemberg through bwHPC (bwunicluster and JUSTUS, RV bw17D011). Financial support from the Helmholtz Association is also gratefully acknowledged.

REFERENCES

1. Cheng, W.-C.; Habib Jr., E. T.; Rajagopalan, K.; Roberie, T. G.; Wormsbecher, R. F.; Ziebarth, M. S., Fluid Catalytic Cracking. In *Handbook of Heterogeneous Catalysis*, pp 2741-2778.
2. Stern, D. L.; Brown, S. H.; Beck, J. S., Isomerization and Transalkylation of Alkylaromatics. In *Handbook of Heterogeneous Catalysis*, pp 3168-3194.
3. Spivey, J. J., Review: Dehydration Catalysts for the Methanol/Dimethyl Ether Reaction. *Chem. Eng. Commun.* **2010**, *110* (1), 123-142.
4. Hemelsoet, K.; Van der Mynsbrugge, J.; De Wispelaere, K.; Waroquier, M.; Van Speybroeck, V., Unraveling the reaction mechanisms governing methanol-to-olefins catalysis by theory and experiment. *ChemPhysChem* **2013**, *14* (8), 1526-45.
5. Olsbye, U.; Svelle, S.; Bjorgen, M.; Beato, P.; Janssens, T. V.; Joensen, F.; Bordiga, S.; Lillerud, K. P., Conversion of methanol to hydrocarbons: how zeolite cavity and pore size controls product selectivity. *Angew. Chem. Int. Ed. Engl.* **2012**, *51* (24), 5810-31.
6. Stöcker, M., Methanol-to-hydrocarbons: catalytic materials and their behavior. *Microporous Mesoporous Mater.* **1999**, *29* (1-2), 3-48.
7. Olsbye, U.; Svelle, S.; Lillerud, K. P.; Wei, Z. H.; Chen, Y. Y.; Li, J. F.; Wang, J. G.; Fan, W. B., The formation and degradation of active species during methanol conversion over protonated zeotype catalysts. *Chem. Soc. Rev.* **2015**, *44* (20), 7155-76.
8. Ghorbanpour, A.; Rimer, J. D.; Grabow, L. C., Periodic, vdW-corrected density functional theory investigation of the effect of Al siting in H-ZSM-5 on chemisorption properties and site-specific acidity. *Catal. Commun.* **2014**, *52*, 98-102.
9. Ghorbanpour, A.; Rimer, J. D.; Grabow, L. C., Computational Assessment of the Dominant Factors Governing the Mechanism of Methanol Dehydration over H-ZSM-5 with Heterogeneous Aluminum Distribution. *ACS Catal.* **2016**, *6* (4), 2287-2298.
10. Di Iorio, J. R.; Gounder, R., Controlling the Isolation and Pairing of Aluminum in Chabazite Zeolites Using Mixtures of Organic and Inorganic Structure-Directing Agents. *Chem. Mater.* **2016**, *28* (7), 2236-2247.
11. Di Iorio, J. R.; Nimlos, C. T.; Gounder, R., Introducing Catalytic Diversity into Single-Site Chabazite Zeolites of Fixed Composition via Synthetic Control of Active Site Proximity. *ACS Catal.* **2017**, *7* (10), 6663-6674.
12. Nystrom, S.; Hoffman, A.; Hibbitts, D., Tuning Brønsted Acid Strength by Altering Site Proximity in CHA Framework Zeolites. *ACS Catal.* **2018**, *8* (9), 7842-7860.
13. Van Speybroeck, V.; Hemelsoet, K.; Joos, L.; Waroquier, M.; Bell, R. G.; Catlow, C. R., Advances in theory and their application within the field of zeolite chemistry. *Chem. Soc. Rev.* **2015**, *44* (20), 7044-111.
14. Svelle, S.; Tuma, C.; Rozanska, X.; Kerber, T.; Sauer, J., Quantum Chemical Modeling of Zeolite-Catalyzed Methylation Reactions: Toward Chemical Accuracy for Barriers. *J. Am. Chem. Soc.* **2009**, *131* (2), 816-25.
15. Bucko, T.; Benco, L.; Dubay, O.; Dellago, C.; Hafner, J., Mechanism of alkane dehydrogenation catalyzed by acidic zeolites: Ab initio transition path sampling. *J. Chem. Phys.* **2009**, *131* (21), 214508.
16. Göttl, F.; Buló, R. E.; Hafner, J.; Sautet, P., What Makes Copper-Exchanged SSZ-13 Zeolite Efficient at Cleaning Car Exhaust Gases? *J. Phys. Chem. Lett.* **2013**, *4* (14), 2244-2249.
17. Paolucci, C.; Parekh, A. A.; Khurana, I.; Di Iorio, J. R.; Li, H.; Albarracín Caballero, J. D.; Shih, A. J.; Anggara, T.; Delgass, W. N.; Miller, J. T. et al. Catalysis in a Cage: Condition-Dependent Speciation and Dynamics of Exchanged Cu Cations in SSZ-13 Zeolites. *J. Am. Chem. Soc.* **2016**, *138* (18), 6028-48.
18. Plessow, P. N.; Studt, F., Unraveling the Mechanism of the Initiation Reaction of the Methanol to Olefins Process Using ab Initio and DFT Calculations. *ACS Catal.* **2017**, *7* (11), 7987-7994.
19. DeLuca, M.; Kravchenko, P.; Hoffman, A.; Hibbitts, D., Mechanism and Kinetics of Methylating C6-C12 Methylbenzenes with Methanol and Dimethyl Ether in H-MFI Zeolites. *ACS Catal.* **2019**, *9* (7), 6444-6460.
20. Brogaard, R. Y.; Henry, R.; Schuurman, Y.; Medford, A. J.; Moses, P. G.; Beato, P.; Svelle, S.; Nørskov, J. K.; Olsbye, U., Methanol-to-hydrocarbons conversion: The alkene methylation pathway. *J. Catal.* **2014**, *314*, 159-169.
21. Yang, G.; Pidko, E. A.; Hensen, E. J. M., Mechanism of Brønsted acid-catalyzed conversion of carbohydrates. *J. Catal.* **2012**, *295*, 122-132.
22. Wang, C.-M.; Wang, Y.-D.; Xie, Z.-K., Verification of the dual cycle mechanism for methanol-to-olefin conversion in HSAPO-34: a methylbenzene-based cycle from DFT calculations. *Catal. Sci. Technol.* **2014**, *4* (8), 2631-2638.
23. Wang, C.-M.; Wang, Y.-D.; Du, Y.-J.; Yang, G.; Xie, Z.-K., Computational insights into the reaction mechanism of methanol-to-olefins conversion in H-ZSM-5: nature of hydrocarbon pool. *Catal. Sci. Technol.* **2016**, *6* (9), 3279-3288.
24. Hoffman, A. J.; Bates, J. S.; Di Iorio, J. R.; Nystrom, S. V.; Nimlos, C. T.; Gounder, R.; Hibbitts, D., Rigid Arrangements of Ionic Charge in Zeolite Frameworks Conferred by Specific Aluminum Distributions Preferentially Stabilize Alkanol Dehydration Transition States. *Angew. Chem. Int. Ed. Engl.* **2020**, *59* (42), 18686-18694.
25. Muller, S.; Liu, Y.; Kirchberger, F. M.; Tonigold, M.; Sanchez-Sanchez, M.; Lercher, J. A., Hydrogen Transfer Pathways during Zeolite Catalyzed Methanol Conversion to Hydrocarbons. *J. Am. Chem. Soc.* **2016**, *138* (49), 15994-16003.
26. Liu, Y.; Kirchberger, F. M.; Muller, S.; Eder, M.; Tonigold, M.; Sanchez-Sanchez, M.; Lercher, J. A., Critical role of formaldehyde during methanol conversion to hydrocarbons. *Nat. Commun.* **2019**, *10* (1), 1462.

27. Carr, R. T.; Neurock, M.; Iglesia, E., Catalytic consequences of acid strength in the conversion of methanol to dimethyl ether. *J. Catal.* **2011**, *278* (1), 78-93.
28. Jones, A. J.; Iglesia, E., Kinetic, spectroscopic, and theoretical assessment of associative and dissociative methanol dehydration routes in zeolites. *Angew. Chem. Int. Ed. Engl.* **2014**, *53* (45), 12177-81.
29. Blaszkowski, S. R.; vanSanten, R. A., Theoretical study of the mechanism of surface methoxy and dimethyl ether formation from methanol catalyzed by zeolitic protons. *J. Phys. Chem. B* **1997**, *101* (13), 2292-2305.
30. Moses, P. G.; Nørskov, J. K., Methanol to Dimethyl Ether over ZSM-22: A Periodic Density Functional Theory Study. *ACS Catal.* **2013**, *3* (4), 735-745.
31. Blaszkowski, S. R.; vanSanten, R. A., The mechanism of dimethyl ether formation from methanol catalyzed by zeolitic protons. *J. Am. Chem. Soc.* **1996**, *118* (21), 5152-5153.
32. Shah, R.; Gale, J. D.; Payne, M. C., In situ study of reactive intermediates of methanol in zeolites from first principles calculations. *J. Phys. Chem. B* **1997**, *101* (24), 4787-4797.
33. Sandre, E.; Payne, M. C.; Gale, J. D., First principles location of the transition state for formation of dimethyl ether in a zeolite. *Chem. Commun.* **1998**, (22), 2445-2446.
34. Jones, A. J.; Carr, R. T.; Zones, S. I.; Iglesia, E., Acid strength and solvation in catalysis by MFI zeolites and effects of the identity, concentration and location of framework heteroatoms. *J. Catal.* **2014**, *312*, 58-68.
35. Migliori, M.; Aloise, A.; Catizzone, E.; Giordano, G., Kinetic Analysis of Methanol to Dimethyl Ether Reaction over H-MFI Catalyst. *Ind. Eng. Chem. Res.* **2014**, *53* (38), 14885-14891.
36. Arvidsson, A. A.; Plessow, P. N.; Studt, F.; Hellman, A., Influence of Acidity on the Methanol-to-DME Reaction in Zeotypes: A First Principles-Based Microkinetic Study. *J. Phys. Chem. C* **2020**, *124* (27), 14658-14663.
37. Goncalves, T. J.; Plessow, P. N.; Studt, F., On the Accuracy of Density Functional Theory in Zeolite Catalysis. *ChemCatChem* **2019**, *11* (17), 4368-4376.
38. Kresse, G.; Furthmüller, J., Efficient iterative schemes for ab initio total-energy calculations using a plane-wave basis set. *Phys. Rev. B* **1996**, *54* (16), 11169-11186.
39. Kresse, G.; Joubert, D., From ultrasoft pseudopotentials to the projector augmented-wave method. *Phys. Rev. B* **1999**, *59* (3), 1758-1775.
40. Perdew, J. P.; Burke, K.; Ernzerhof, M., Generalized Gradient Approximation Made Simple *Phys. Rev. Lett.* **1997**, *78*, 1396-1396.
41. Grimme, S.; Antony, J.; Ehrlich, S.; Krieg, H., A Consistent and Accurate Ab Initio Parametrization of Density Functional Dispersion Correction (DFT-D) for the 94 Elements H-Pu. *J. Chem. Phys.* **2010**, *132* (15), 154104.
42. Plessow, P. N., Efficient Transition State Optimization of Periodic Structures through Automated Relaxed Potential Energy Surface Scans. *J. Chem. Theory Comput.* **2018**, *14* (2), 981-990.
43. Fletcher, R. E.; Ling, S.; Slater, B., Violations of Lowenstein's rule in zeolites. *Chem Sci* **2017**, *8* (11), 7483-7491.
44. Knott, B. C.; Nimlos, C. T.; Robichaud, D. J.; Nimlos, M. R.; Kim, S.; Gounder, R., Consideration of the Aluminum Distribution in Zeolites in Theoretical and Experimental Catalysis Research. *ACS Catal.* **2017**, *8* (2), 770-784.
45. Heard, C. J.; Grajciar, L.; Nachtigall, P., The effect of water on the validity of Lowenstein's rule. *Chem Sci* **2019**, *10* (22), 5705-5711.
46. Sun, J.; Fang, H.; Ravikovitch, P. I.; Sholl, D. S., Understanding Dealumination Mechanisms in Protonic and Cationic Zeolites. *J. Phys. Chem. C* **2019**, *124* (1), 668-676.
47. Tang, X.; Liu, Z.; Huang, L.; Chen, W.; Li, C.; Wang, G.; Li, G.; Yi, X.; Zheng, A., Violation or Abidance of Löwenstein's rule in Zeolites Under Synthesis Conditions? *ACS Catal.* **2019**, *9* (12), 10618-10625.
48. Nimlos, C. T.; Hoffman, A. J.; Hur, Y. G.; Lee, B. J.; Di Iorio, J. R.; Hibbitts, D. D.; Gounder, R., Experimental and Theoretical Assessments of Aluminum Proximity in MFI Zeolites and Its Alteration by Organic and Inorganic Structure-Directing Agents. *Chem. Mater.* **2020**, *32* (21), 9277-9298.
49. Fant, M.; Angqvist, M.; Hellman, A.; Erhart, P., To Every Rule There is an Exception: A Rational Extension of Loewenstein's Rule. *Angew. Chem. Int. Ed. Engl.* **2021**, *60* (10), 5132-5135.
50. Ma, S.; Shang, C.; Wang, C.-M.; Liu, Z.-P., Thermodynamic rules for zeolite formation from machine learning based global optimization. *Chemical Science* **2020**, *11* (37), 10113-10118.
51. Plessow, P. N.; Studt, F., How Accurately Do Approximate Density Functionals Predict Trends in Acidic Zeolite Catalysis? *J. Phys. Chem. Lett.* **2020**, *11* (11), 4305-4310.
52. Vansanten, R. A.; Kramer, G. J., Reactivity Theory of Zeolitic Bronsted Acidic Sites. *Chem. Rev.* **1995**, *95* (3), 637-660.
53. Brandle, M.; Sauer, J., Acidity differences between inorganic solids induced by their framework structure. A combined quantum mechanics molecular mechanics ab initio study on zeolites. *J. Am. Chem. Soc.* **1998**, *120* (7), 1556-1570.
54. Bordiga, S.; Regli, L.; Cocina, D.; Lamberti, C.; Bjorgen, M.; Lillerud, K. P., Assessing the acidity of high silica chabazite H-SSZ-13 by FTIR using CO as molecular probe: Comparison with H-SAPO-34. *J. Phys. Chem. B* **2005**, *109* (7), 2779-2784.
55. Wang, C. M.; Brogaard, R. Y.; Weckhuysen, B. M.; Nørskov, J. K.; Studt, F., Reactivity Descriptor in Solid Acid Catalysis: Predicting Turnover Frequencies for Propene Methylation in Zeotypes. *J. Phys. Chem. Lett.* **2014**, *5* (9), 1516-21.
56. Wang, C.-M.; Brogaard, R. Y.; Xie, Z.-K.; Studt, F., Transition-state scaling relations in zeolite catalysis: influence of framework topology and acid-site reactivity. *Catal. Sci. Technol.* **2015**, *5* (5), 2814-2820.
57. Liu, C.; van Santen, R. A.; Poursaeidesfahani, A.; Vlugt, T. J. H.; Pidko, E. A.; Hensen, E. J. M., Hydride Transfer versus Deprotonation Kinetics in the Isobutane-Propene Alkylation Reaction: A Computational Study. *ACS Catal.* **2017**, *7* (12), 8613-8627.

